ISSN NO. 2320-5407

Journal Homepage: - www.journalijar.com

INTERNATIONAL JOURNAL OF ADVANCED RESEARCH (IJAR)

Article DOI: 10.21474/IJAR01/1617
DOI URL: http://dx.doi.org/10.21474/IJAR01/1617

RESEARCH ARTICLE

FINITE ELEMENT SIMULATION OF TEMPERATURE AND CURRENT DISTRIBUTIONS DURING SPARK PLASMA SINTERING (SPS).

Souhir Mankai[1], Jamel Madiouli[1,2] and Jalila Sghaier[1].

1. Department of Energy Engineering, National Engineering School of Monastir, University of Monastir, 5019 Monastir, Tunisia.
2. Mechanical Engineering Department, Faculty of Engineering, King Khalid university, Abha, KSA.

Manuscript Info

Manuscript History

Received: 14 July 2016
Final Accepted: 12 August 2016
Published: September 2016

Keywords: -
Spark Plasma Sintering, modeling, finite element, temperature distribution.

Abstract

A finite element model is elaborated to simulate coupling of thermal and electrical behavior of Spark Plasma Sintering (SPS). the temperature and the current distributions were analysed in the case of two sample materials widely differing electrical conductivities (alumina and titanium aluminide) with thermal properties and electrical temperature-dependent.

Introduction: -

Sintering is the process of compacting and forming a coherent material under the action of heat. this process is used in several domains such as reconstruction of bone defect in maxillofacial, dental and orthopedic applications (Rodriguez-Lorenzo et al., 2003), (Guidara et al., 2011), treatment of nuclear waste (Gong et al., 1999), fabrication of conductive electrodes for several optoelectronic devices (Sun et al., 2010), etc.

Many techniques have been developed; their specificities reside in the way of heating the powder. These techniques include the conventional sintering (also called natural sintering) and non-conventional sintering such as sintering under load (compaction hot uniaxial or hot isostatic pressing), the flash sintering also called SPS (applying an electric current and a uniaxial pressure), the laser sintering (scan a powder bed by a laser beam) and the microwave sintering (irradiation by a microwave field).

In this paper, we will interest to the Spark Plasma Sintering technique which is a novel technique that employs a pulsed direct current and uniaxial pressure to ameliorate consolidation. Compared to conventional sintering, the SPS process has numerous benefits such as shortened processing time, reduced sintering temperature and making it possible to manufacture nano-structured materials highly densified.

In last one decade, researches on the SPS technology have continued to grow if one refers to the number of publications on the subject (Pavia, 2012). Much of this work is experimental (Zehani, 2013), but more experiments are accompanied by finite element simulation (Vanmeensel et al. 2005), (Maizza et al., 2007), to determine the material properties which is difficult to obtain experimentally.

Corresponding Author:- Souhir Mankai
Address:- Department of Energy Engineering, National Engineering School of Monastir, University of Monastir, 5019 Monastir, Tunisia.

Recently commercial calculation codes were used for these simulations. Zavaliangos et al. (2004) has developed a thermo-electrical model and used the 'Abaqus' code to study the contact resistance problem. Wang et al. (2010) has simulated by 'Comsol' the thermo-electo-mechanical model of SPS process.

In this article, a thermo-electical modeling of sintering SPS is developed. In the first part, we present the SPS machine and the thermo-electrical model is detailed, then the results are presented and analyzed.

Modeling: -

The finite element modelling is based on a set of governing equations that involve a dynamic coupling of the Fourier's law and the charge conservation equation. The coupling between temperature and electrical potential is strong because of the high dependence of thermal and electrical coefficients on the temperature.

To reduce the unnecessary complexity of modelling, some simplifications are taken into account:
both graphite, alumina (Al_2O_3) and titanium aluminide (TiAl) powder compact are treated as isotropic
Only one half of the system domain cross section is required for modelling because of the axial symmetry of the device (the SPS process corresponds to a two-dimensional axisymmetric model)
The geometric dimensions and the main physical properties of graphite, alumina and titanium aluminide are listed in Table 1 and Table2.
The temperature and the electrical potential are governed by the following system of equations:

$$\nabla \vec{J} = 0 \qquad (1)$$

$$\rho c_p \frac{\partial T}{\partial t} + \nabla\left(-\lambda \nabla T\right) = q_e \qquad (2)$$

Where $q_e = \vec{J}.\vec{E}$ is the heat generated by the current per unit volume per unit time, $\vec{J} = \sigma_c \vec{E}$ is the current density and $E = -\nabla\phi$ is the electric field.

The initial and boundary conditions (Fig.2) used for the solutions are:
- The initial temperature is 300 K and the initial voltage is 4V.
- The process takes place in vacuum, so heat losses by convection or conduction through the gas are neglected.
- All the lateral surfaces have heat losses by radiation towards the chamber walls, which are held at room temperature 300 K. This heat loss is given by

$$q_r = \sigma_s \varepsilon \left(T_e^4 - T_a^4\right) \qquad (3)$$

Where ε is the emissivity (which is assumed to be equal to 0.8 for the graphite), σ_s is the Stefan-Boltzmann constant, T_e is the temperature of the die surface (emission surface temperature (graphite)) and T_a is the temperature of the walls of the chamber (absorption surface temperature (chamber walls)).

- A system of water-cooling removes some heat at the electrodes toward the graphite. The equation of conducto-convective heat flow is expressed by:

$$q_c = h_c(T_i - T_w) \qquad (4)$$

Where h_c is the conducto-convective coefficient, T_i is the water temperature and T_w the temperature of the wall in contact with water. Note that the water cooling circuit, which operates directly on all the graphite surfaces, was considered with water at 300K, while in the experimental setup this is achieved by a steel piece containing the cooling system.

- The sides of all equipment are considered as electrically insulate. Voltage is only known at one extreme surface: 0V on the bottom surface and a constant current is applied at the top of the device (I=2100A).

Results and Discussion: -

The temperature distribution during the process (both within the sample and in the die) is an important parameter, as it influences the sample homogeneity. A difference between conducting and non-conducting samples can be observed in the radial temperature distribution (Fig.3). The figure shows the radial temperature distribution at a constant current of 2100 A. The temperature is not constant across the samples, with a significant temperature gradient seen in the case of the non-conducting sample.

Fig.4. shows the changes in the temperature distribution with time for times ranging from 10 to 510s for alumina. The behavior described above is qualitatively the same for the case of conducting samples.

The distribution along the vertical axis influences the radial distribution of the current. This can be seen from Fig.5 which shows the radial distribution for the cases of alumina and TiAl samples. For the non-conducting sample, no current is carried by the sample and the current has a relatively low gradient from the inside of the die to the outside, with the highest current density being close to the sample surface (the inside surface of the die). In contrast, for the conducting sample, the radial current distribution is more complex. The current density decreases in the inside of the sample to a minimum value, becomes the highest at the lateral surface of the sample then decreases steeply in the graphite and remains relatively constant beyond that.
To conclude, we can say that the electrical conductivity can significantly affect the temperature uniformity and the current distribution.

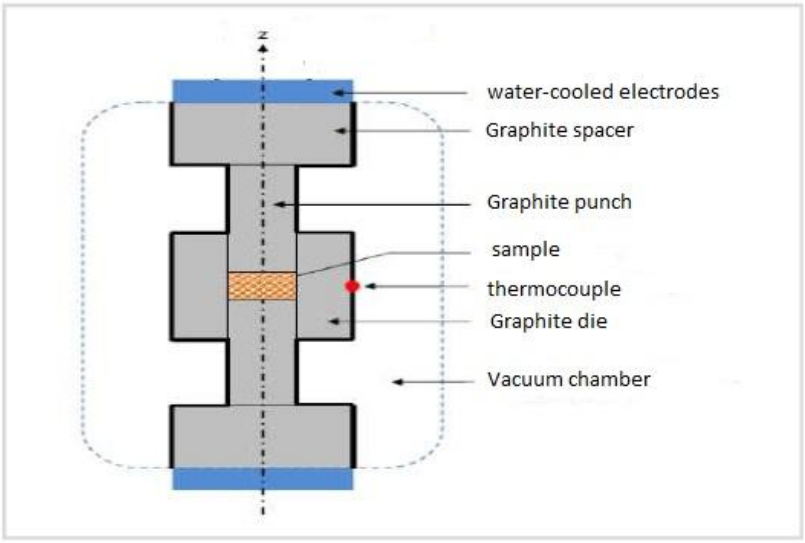

Fig.1: - Schematic of the SPS apparatus

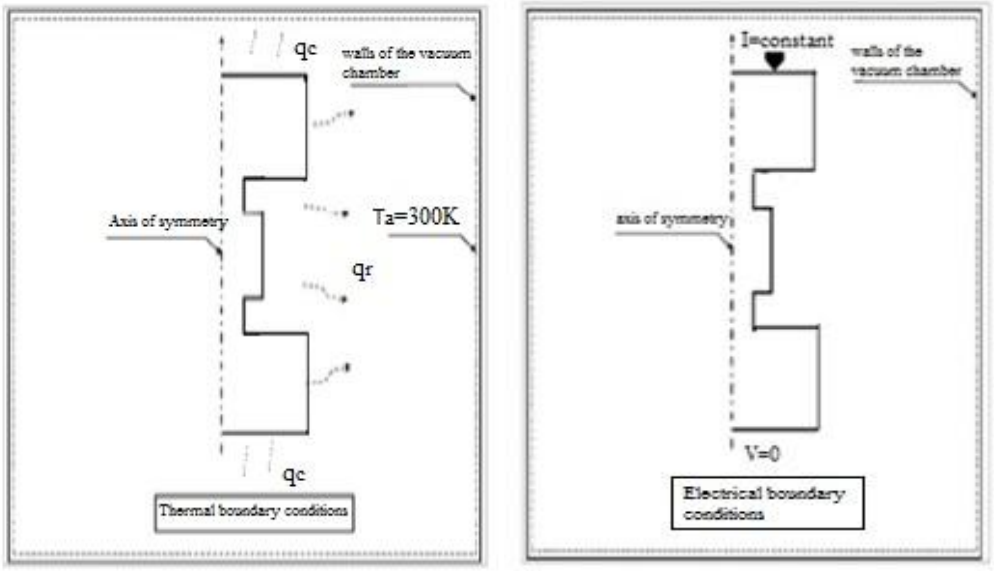

(a) (b)

Fig.2: - Thermal and electrical boundary conditions applied to the model

Table 1: - The geometric dimensions of the apparatus

Dimension	Diameter (m)	Height (m)
Sample	0.02	0.005
Die	0.04	0.048
Punch	0.02	0.035
Spacer	0.08	0.045

Table 2: - The properties of the graphite, the alumina and the titanium aluminide

		Al_2O_3	TiAl	Graphite
Density	ρ (kg/m^3)	3900	3900	1850
Thermal conductivity	λ (W/m.K)	$39500*T^{-1.26}$	411*exp(−0.0025T)	-0.017T+65
Electric resistivity	ρ_e (Ω.m)	$8.7*10^{19}*T^{-4.82}$	4.5*exp(−0.0027T)	$26-3*10^{-2}T+2*10^{-5}T^2-6.4*10^{-9}T^3+7.8*10^{-13}T^4$
Heat capacity	C_p (J/kg.K)	850	670	1.7T+310.5

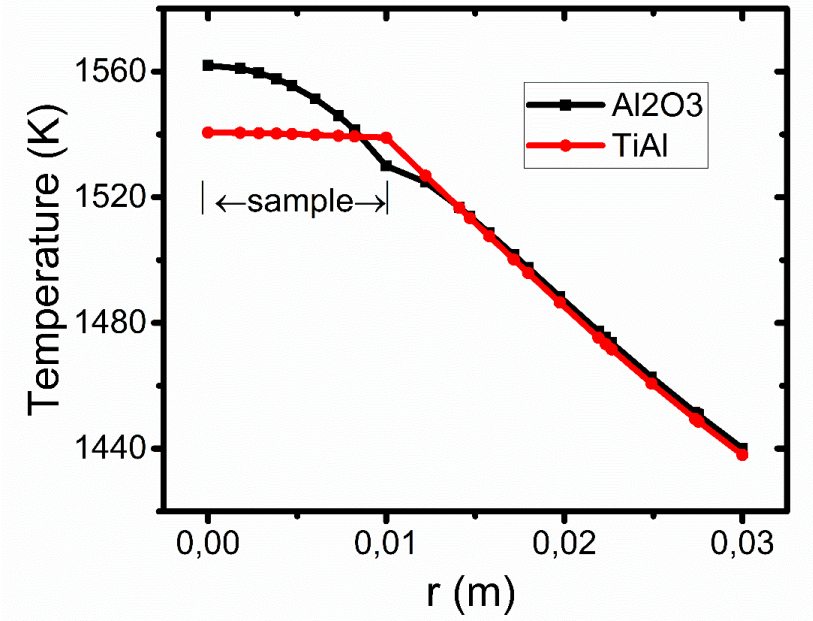

Fig.3: - Calculated radial temperature distributions for non-conducting (Al_2O_3) and conducting (TiAl) samples (z=0)

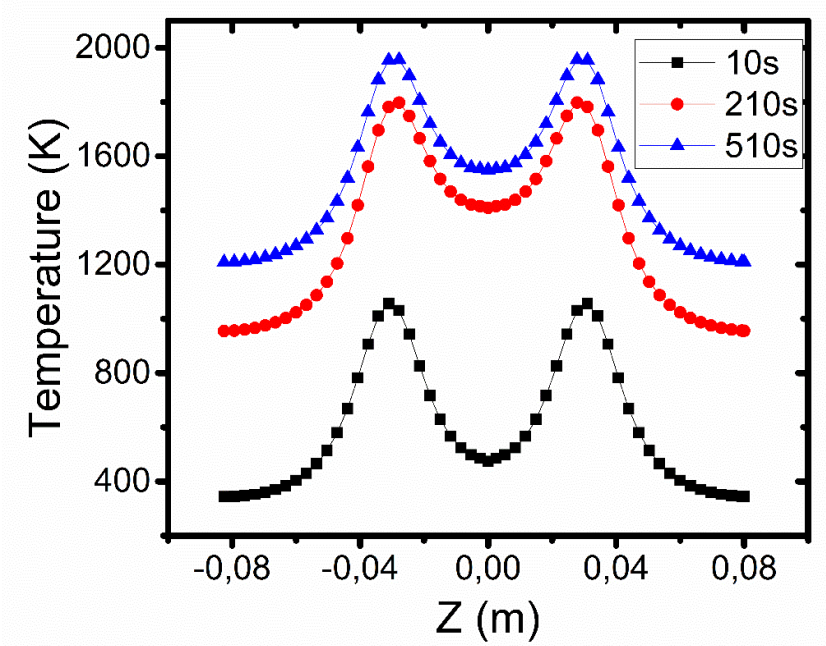

Fig. 4: - Calculated temperature distribution of alumina sample along the vertical axis for different Times (r=0)

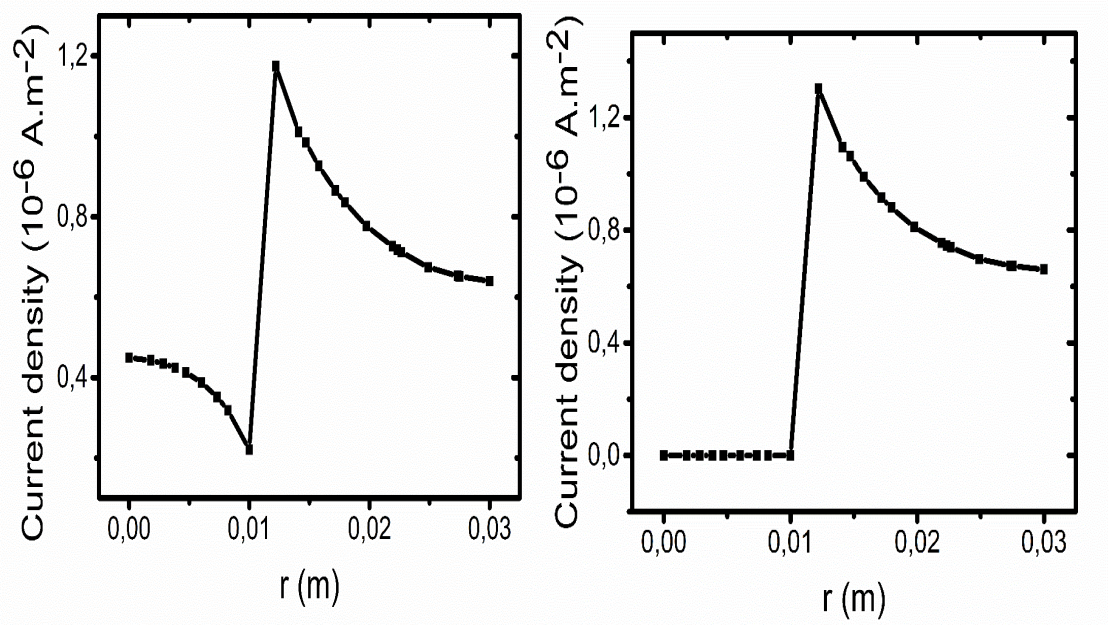

(a) (b)

Fig. 5: - Radial current density distribution for: (a) conducting (TiAl) and (b) non-conducting (Al_2O_3) and samples (z=0)

Conclusion: -

In this study, a numerical model used the finite element simulation was constructed. The temperature and the current distribution were evaluated in the radial and axial directions using two samples with a large difference in electrical conductivity (alumina and titanium aluminide). A difference between the shape of the curves for the two products is seen, this allow us to conclude that the temperature and the current distributions are strongly dependent on the electrical conductivity of the sample.

References: -

1. **Rodriguez-Lorenzo, L. M., Hart, J. N., Gross, K. A (2003).** Influence of Fluorine in the Synthesis of Apatites. Syn-thesis of Solid Solutions of Hydroxyl-Fluorapatite. Biomaterials. 24: 3777-3785.
2. **Guidara, A., Chaari, K. and Bouaziz, J. (2011).** Elaboration and characterization of alumina-fluorapatite composites. J Biomater Nanobiotechnol. 2: 103-113.
3. **Gong, W., Lutze, W.F, Abdelouas, A., Ewing, R.C. (1999)**. Vitrification of radioactive waste by sintering under pressure. J Nucl Mater. 265 (1):12-21.
4. **Sun,Y.H., Xiong, W.H., Li, C.H. (2010)**. Fabrication of ultrahigh density ZnO-Al2O3, ceramic composites by slip casting. T Nonferr Metal Soc. 20 (4) : 624-631
5. **Pavia, A. (2012).** Études fondamentales pour la compréhension des mécanismes de densification des matériaux par la technologie Spark Plasma Sintering. Ph.D. Thesis, Université Toulouse III Paul Sabatier (UT3 Paul Sabatier).
6. **Zehani, K. (2011).** Etude du ferrite NiZnCu nanostructuré produit par SPS : des propriétés physiques à la réalisation de composants monolithiques intégrés. Ph.D. Thesis, Université Paris Saclay.
7. **Vanmeensel, K., Laptev, A., Hennicke, J., Vleugels, J., Vander Biest, O. (2005).** Modeling of the temperature distribution during field assisted sintering. Acta Mater. 53, 4379-4388.
8. **Maizza, G., Grasso, S., Sakka, Y., Noda, T., Ohashi, O. (2007).** Relation between microstructure, properties and spark plasma sintering (SPS) parameters of pure ultrafine WC powder. Sci. Technol Adv. Mater. 8: 644-654.
9. **Zavaliangos, A., Zhang, J., Krammer, M., Groza, J.R. (2004).** Temperature evolution during field activated sintering. Mater Sci Eng A. 379: 218–228.
10. **Wang, C., Cheng, L., Zhao, Z. (2010).** FEM analysis of the temperature and stress distribution in spark plasma sintering: Modelling and experimental validation. Computational Materials Science. 49: 351–362.